# Channel Activity of OmpF Monitored in Nano-BLMs

Eva K. Schmitt,* Maarten Vrouenraets,† and Claudia Steinem*
*Institut für Analytische Chemie, Chemo- und Biosensorik, Universität Regensburg, 93040 Regensburg, Germany; and †Biomade Technology Foundation, 9747 AG Groningen, The Netherlands

ABSTRACT Free-standing lipid bilayer membranes can be formed on small apertures (60 nm diameter) on highly ordered porous alumina substrates. The formation process of the membranes on a 1,2-dipalmitoyl-*sn*-glycero-3-phosphothioethanol submonolayer was followed by impedance spectroscopy. After lipid bilayers had thinned, the reconstitution and ionic conducting properties of the outer membrane protein OmpF of *E. coli* were monitored using single-channel recordings. The characteristic conductance states of the three monomers, fast kinetics, and subconductance states were observed. Blockade of the ion flow as a result of interaction of the antibiotic ampicillin with the protein was verified, indicating the full functionality of the protein channel in nanometer-scale bilayer membranes.

## INTRODUCTION

Many pharmaceutical drugs are intended to act on ion channels and transporters that are located in a biological membrane. Planar lipid membranes spanning a small hole, ~0.1–1 mm in diameter, in thin Teflon films were developed to electrically follow the function of those proteins (1,2). Even though these membranes are well established, they do not allow for integration, automation, parallelization, and applications on a micro- or nanometer scale as required for the development of screening systems for ion channels and transporters. Because there is a lively interest in screening systems operated with chip technology demanding easy handling and reliable processes, new strategies have been developed in recent years. Silicon or glass chips with 0.7–100-$\mu$m-large apertures served as supports for lipid membranes suspending a single hole (3–7). These membranes were prepared in various ways such as painting lipids dissolved in organic solvents across the aperture or spreading vesicles. However, the long-term and mechanical stability reported for the free-standing membranes averaged only several hours.

The stability of membranes is essential for an application in automated screening processes. This requirement is met by lipid bilayers immobilized on solid supports (8–11). To establish solid supported membranes (SSMs), either two separate monolayers can be deposited on the material by means of the Langmuir-Blodgett or Langmuir-Schäfer technique, or, more easily, self-assembly processes are exploited. The advantage of a high mechanical stability of SSMs is at the expense of a lack of a second aqueous compartment, which hampers the electrical investigation of ion channel proteins. Furthermore, interactions of transmembrane protein domains with the solid support might significantly alter their properties. Alternative systems with hydrophilic spacer molecules attached to the surface separating the bilayer from the solid support by 1–3 nm, known as tethered membranes, reduce this interaction and provide a small aqueous compartment (8,12,13). Recently, tethered membranes with good electrical sealing properties were successfully prepared and made it possible to measure ion flow through reconstituted ion channels (14,15).

More recently, we established an artificial membrane system that combines the advantages of SSMs with the need for a second aqueous compartment to elucidate channel properties of complex integral membrane proteins (16,17). Porous alumina substrates with highly ordered pores of 60 and 280 nm in diameter, respectively, were functionalized with lipid bilayers suspending the pores of the porous material, which we called nano-black lipid membranes (nano-BLMs). Nano-BLMs are characterized by a high membrane resistance and thus proved to be well suited for an application in single-channel recordings on peptide ion channels (17). Furthermore, nano-BLMs allowed for the investigation of the proton pump bacteriorhodopsin (18).

Relatively large transmembrane proteins such as $\alpha$-hemolysin (19) and the glutamate receptor (20) have been reconstituted into membranes on orifices in either polycarbonates or silicon with diameters greater than 1 $\mu$m. We raised the question of how the pore size of the porous material limits the incorporation and the functionality of a complex integral membrane protein in pore-suspending membranes. To address this question, the functional insertion of the outer membrane protein OmpF of *E. coli* was investigated in nano-BLMs on porous alumina with a pore diameter of 60 nm by observing the ion channel activity in single-channel recordings. OmpF was chosen because it is well characterized in terms of structure (21,22) and channel activity. It is composed of 16 antiparallel aligned $\beta$-sheets ($\beta$-barrel) connected by amino acid sequences referred to as loops and turns, building up a water-filled pore. Three of these monomeric units with a molecular weight of 37.1 kDa (22) and a length

*Submitted February 18, 2006, and accepted for publication June 5, 2006.*

Address reprint requests to Claudia Steinem, Institut für Analytische Chemie, Chemo- und Biosensorik, Universität Regensburg, 93040 Regensburg, Germany. Tel.: 49-941-943-4548; Fax: 49-941-943-4491; E-mail: claudia.steinem@chemie.uni-regensburg.de.



0006-3495/06/09/2163/09 $2.00

doi: 10.1529/biophysj.106.083592

of 5 nm (21) are arranged around a threefold molecular axis. Loop 3 (L3) folds into the barrel, forming a constriction zone of (11 × 7) $Å^2$ at approximately half the height of the channel. Positively charged residues of L3 and negatively charged amino acids of the inner barrel wall are postulated to be the origin of a strong transverse electric field (23,24). The constriction zone is assumed to be a decisive factor regarding conductivity and ion selectivity as elucidated by means of computer simulations and mutant studies (25–28). OmpF is slightly cation selective ($Li^+ < Na^+ < K^+$) (23) and permeable for hydrophilic molecules up to 600 Da. External parameters such as pH, ionic strength, and membrane potential significantly influence the ion permeability (29–32). At a critical voltage the channel closes completely, although the value of the potential necessary to induce this phenomenon varies considerably (30,31,33,34). Information about the molecular basis of voltage gating was recently obtained in computational studies assessing the constriction zone, which plays a crucial role in the process (35).

Despite the substantial role of computer-based studies on OmpF, electrical methods are required to understand the channel properties. To perform such measurements, the protein is either inserted in classical BLMs and investigated by the voltage-clamp method or studied in giant liposomes as well as membrane fractions by means of the patch-clamp technique (30,36–38). With these methods, only recently, the phenomenon of subconductance states has been investigated thoroughly (39). Furthermore, there is great interest in how specific molecules influence the ion permeability of the pore. Small molecules such as polyamines or $\beta$-lactams, i.e., ampicillin, block the ion flow through the pore temporarily, leading to a fast flickering of the channel activity as monitored in voltage-clamp experiments (40–42), which was corroborated by computational studies (42,43).

Here, we raised the question whether such a large protein with an area of roughly 80 $nm^2$ embedded within a pore that is covered by only a few thousand lipids is still fully functional or if the supported part of the membrane on the pore rims influences its activity. The study demonstrates that all the characteristic properties of the OmpF channel, including blockade by ampicillin, can be observed in nano-BLMs.

## MATERIALS AND METHODS

### Materials

Aluminum substrates (thickness 0.5 mm, purity 99.999%) were purchased from Goodfellow (Huntington, UK). The lipids 1,2-dipalmitoyl-*sn*-glycero-3-phosphothioethanol (DPPTE) and 1,2-diphytanoyl-*sn*-glycero-3-phosphocholine (DPhPC) were obtained from Avanti Polar Lipids (Alabaster, AL). Ampicillin sodium salt (purity 99%) was purchased from Carl Roth GmbH (Karlsruhe, Germany), octyl-polyoxyethylene (o-POE) from Bachem (Bubendorf, Germany), and *n*-decane from Sigma-Aldrich (Taufkirchen, Germany). The protein OmpF was a kind gift from BioMade (Groningen, The Netherlands). The water used was ion-exchanged and filtered with a Milli-Q-System (Millipore, Molsheim, France; specific resistance $R > 18$ $M\Omega\ cm^{-1}$, pH 5.5).

### Preparation and functionalization of porous alumina substrates

A detailed procedure for the preparation of porous alumina substrates is described elsewhere (17). Briefly, the aluminum foils were cleaned with ethanol, electropolished, and anodized in aqueous 0.3 M oxalic acid solution at $U = 40$ V and $T = 2°C$ for 5 d. The resulting porous alumina substrates were then incubated with a saturated $HgCl_2$-solution to remove the underlying aluminum layer. Pore bottoms were removed by chemical etching at $T = 30°C$ with 10 wt % phosphoric acid solution, and the bottom surface was coated with a thin 25-nm gold layer using a sputter coater with a thickness control unit (Cressington sputter coater 108auto, Cressington MTM-20, Elektronen-Optik-Service, Dortmund, Germany). The gold-coated substrates were functionalized with DPPTE (0.5 mM ethanolic solution, $t > 12$ h). After thorough rinsing with ethanol, the resulting hydrophobic porous samples were mounted vertically in a Teflon cell (Fig. 1), which was used for both impedance analysis and single-channel recordings.

### Formation of nano-BLMs and reconstitution of OmpF

The *cis* and *trans* compartments of the Teflon cell were filled with 8.5 ml electrolyte solution composed of 1 M KCl, 1 mM $CaCl_2$, pH 6.0, and 8.5 $\mu$l of a solution of 1,2-diphytanoyl-*sn*-glycero-3-phosphocholine (DPhPC) (2% w/v) in *n*-decane was applied to the surface of the functionalized porous

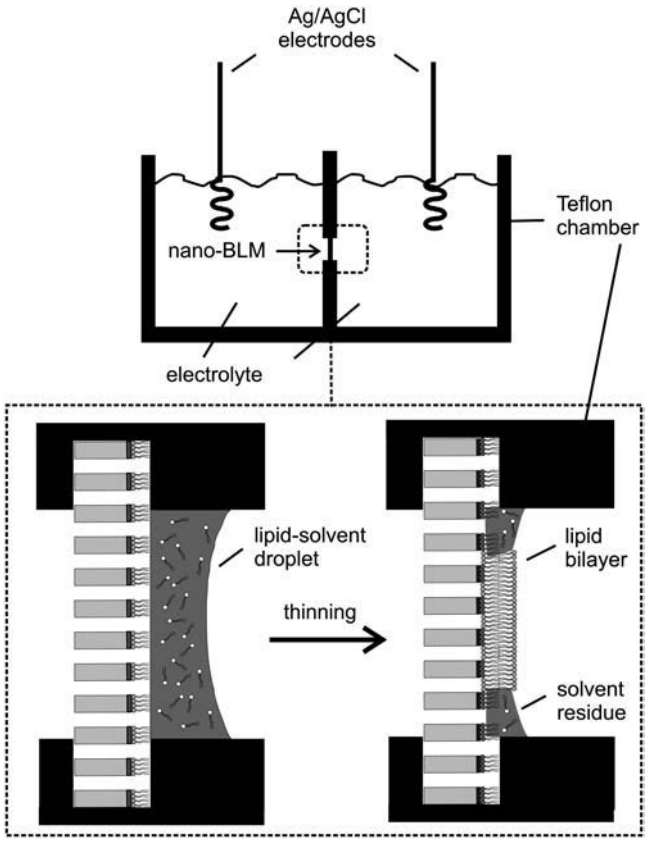


FIGURE 1 Setup of the measuring chamber. The porous material is fixed vertically between two Teflon chambers. A membrane is created by applying a lipid-solvent droplet on the porous substrate. The spontaneous thinning of the lipid-solvent droplet to a lipid bilayer is depicted in the enlarged part of the chamber. The resulting membrane spans the pores.

substrate. After impedance analysis of the formed nano-BLM, 1–5 $\mu$l of a 1 $\mu$g/ml OmpF solution (1% v/v o-POE) was added to the *cis*-side of the cell, leading to a final concentration of 0.06–0.3 ng/ml. To investigate the influence of ampicillin on OmpF, 6 mM ampicillin was added to the buffer. The ampicillin solution was stored at 8°C to avoid polymerization of the molecules.

### Impedance spectroscopy

Lipid membranes and their formation process on the porous substrates were characterized by impedance spectroscopy using the gain/phase analyzer SI 1260 and the 1296 Dielectric Interface (Solartron Instruments, Farnborough, UK). The measurements were controlled by a personal computer. The membrane formation process was observed time-resolved by reading out the absolute value of the impedance $|Z|(f)$ and the phase angle between current and voltage $\phi(f)$ at a constant frequency of $10^6$ Hz. Impedance spectra ($|Z|(f)$, $\phi(f)$) were recorded in a frequency range of $10^{-3}$–$10^6$ Hz, which took ~35 min. Platinized platinum wires served as working and counter electrodes. All data points were obtained at zero offset potential applying an AC voltage of 30 mV. The Solartron Impedance Measurement Software (version 3.5.0) was used for data recording, the software package Zview2.6b with Calc-Modulus data weighting for data analysis.

### Channel current recordings

For channel recordings, the Teflon cell with the nano-BLM was placed in a Faraday cage to avoid interference from electric fields during measurements. Two Ag/AgCl wires served as electrodes. The *trans* compartment was connected to ground, and all potentials in the *cis* compartment are given relative to ground. Currents were recorded with an Axopatch 200B patch-clamp amplifier (Axon Instruments, Foster City, CA). The analog output signals were filtered with a low-pass four-pole Bessel filter of 1 kHz and subsequently digitized by an A/D converter (Digidata 1322, Axon Instruments). The sampling rate was 50 kHz. The recordings in the presence of ampicillin were carried out with a filter of 2 kHz, and data were acquired at 200 kHz. The software package pClamp9.2 (Axon Instruments) was employed to control data recording and for analysis. For all measurements, the applied potential was clamped at $U = -100$ mV. Measurements were carried out in a symmetrical nonbuffered electrolyte solution composed of 1 M KCl, 1 mM $CaCl_2$, pH 6.0. OmpF was added at the *cis*-side.

## RESULTS

### Impedance analysis of the formation of nano-BLMs

For the formation of nano-BLMs, highly ordered porous alumina substrates were used with a mean pore diameter of 60 nm. After spreading 8.5 $\mu$l DPhPC (2% w/v) dissolved in *n*-decane on the porous substrate, we followed the process of membrane formation in 1 M KCl, 1 mM $CaCl_2$, pH 6.0 by means of impedance spectroscopy. In Fig. 1, a schematic drawing of the thinning process and the lipid bilayers suspending the pores of the porous alumina substrate, which is in a vertical position between two Teflon chambers, is shown. In a previous work the formation of pore-spanning membranes was investigated by monitoring the membrane capacitance $C_m$ time-dependently after painting a lipid droplet on the porous substrate. The increase in capacitance over a period of ~10–25 min was interpreted as a thinning process of the lipid bilayer (17). To obtain a better time resolution, here the thinning process was followed time-resolved at a fixed frequency of $10^6$ Hz. Fig. 2, *A* and *B* display the absolute value of the impedance $|Z|(f)$ and the phase angle $\phi(f)$ directly after the painting of a lipid droplet across the substrate as well as spectra of a lipid bilayer after the thinning process.

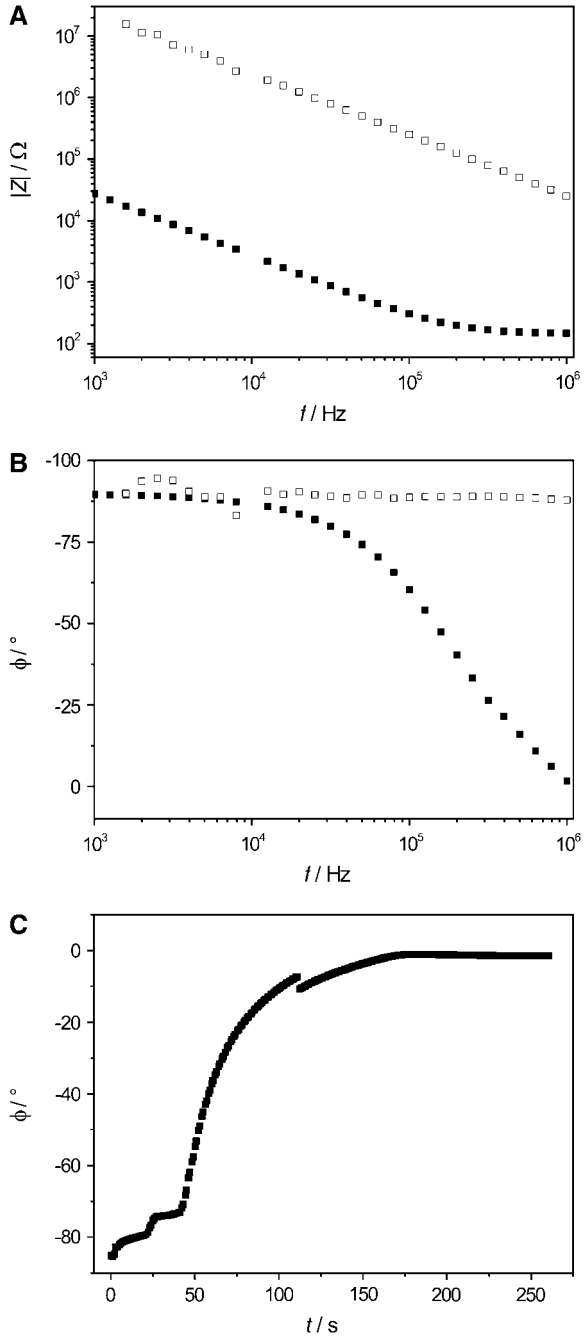


FIGURE 2 (*A*) Typical recording of the absolute value of the impedance $|Z|(f)$ and (*B*) phase angle $\phi(f)$ monitored for a lipid droplet immediately after its application on the porous substrate (□) and after the thinning process (■). The difference between the spectra is most significant at $10^6$ Hz. (*C*) Time-resolved increase in $\phi(f)$ during the membrane formation makes it possible to follow the kinetics and the completeness of the thinning process. Electrolyte: 1 M KCl, 1 mM $CaCl_2$, pH 6.0.

At a frequency of $10^6$ Hz, $|Z|(f)$ and $\phi(f)$ before and after thinning differ significantly. The absolute value of the impedance of the system with a fully established bilayer is frequency-independent at $10^6$ Hz, whereas immediately after lipid application, a capacitance is predominant, and thus, a phase shift of around $-90°$ is detected. Measuring $\phi$ at a frequency of $10^6$ Hz allows the kinetics of the thinning process to be monitored with high time resolution. Fig. 2 *C* illustrates the shift of the phase angle $\phi(10^6$ Hz) from $-85°$ after lipid application to almost 0° after 150 s. The small increases in $\phi(10^6$ Hz) within the first 50 s followed by a fast one to a value close to 0° was observed in >50% of all measurements. Sometimes, within the time course, sudden small drops of the phase angle, as also observed in the time course depicted in Fig. 2 *C* after 110 s, were monitored. As a first approximation, a monoexponential function was fit to the data in the time regime of 50–200 s, resulting in a time constant of $\tau = 28$ s.

After the thinning process had been completed, impedance spectra within a frequency range of $10^{-3}$–$10^6$ Hz were taken, and an equivalent circuit composed of a parallel connection of a capacitance $C_m$ and a resistance $R_m$ in series to an ohmic resistance representing the electrolyte resistance was fit to the data. A good accordance between data and fit was achieved resulting in a mean specific membrane capacitance $C_m = 0.4 \pm 0.1$ $\mu$F/cm$^2$ as calculated from 18 independent experiments taking the porous area into account (17). This value is in good agreement with specific capacitance values obtained from classical BLMs generated by the Müller-Rudin technique, which are reported to be around 0.5 $\mu$F/cm$^2$ (44).

The membrane capacitance is an invaluable parameter to control and evaluate the process of nano-BLM formation. The second characteristic parameter is the membrane resistance $R_m$, which is determined at very low frequencies in the impedance spectrum. A nano-BLM with a membrane resistance of >1 GΩ is essential for its application in single-channel recordings. The resistance of the pore-spanning membranes generated in this work exceeded the critical value of around 1 GΩ in every preparation, which is sufficient for low-conductance measurements. This high membrane resistance of >1 GΩ was monitored during the experimental period of typically 8–10 h.

## Channel activity of OmpF reconstituted in nano-BLMs

Reconstitution of the OmpF channel into the preformed nano-BLMs was achieved by adding the protein in detergent solution to the *cis*-compartment of the Teflon cell. The reconstitution of the trimeric protein into the membrane causes both a three-step increase in conductance and a step decrease in ionic current corresponding to the opening and closing of the channel subunits. A characteristic current trace after insertion of one channel protein in the presence of 1 M KCl, 1 mM $CaCl_2$, pH 6.0 at a holding potential of $U = -100$ mV is depicted in Fig. 3 *A*. The graph indicates the current of the closed state (C) and of the three opening levels ($O_1$, $O_2$, $O_3$). All-point histogram analysis of the current traces allowed the determination of the three different conductance levels with $G_1 = 1700 \pm 80$ pS, $G_2 = 3360 \pm 80$ pS, and $G_3 = 5060 \pm 50$ pS (Fig. 3 *B*). The conductance of one subunit monomer calculated as the difference between the conductance states averages $G_m = 1690 \pm 20$ pS. On occasion, we recorded transient currents as depicted in Fig. 3 *C*. In these events, a sudden increase in current is followed by an exponential decay.

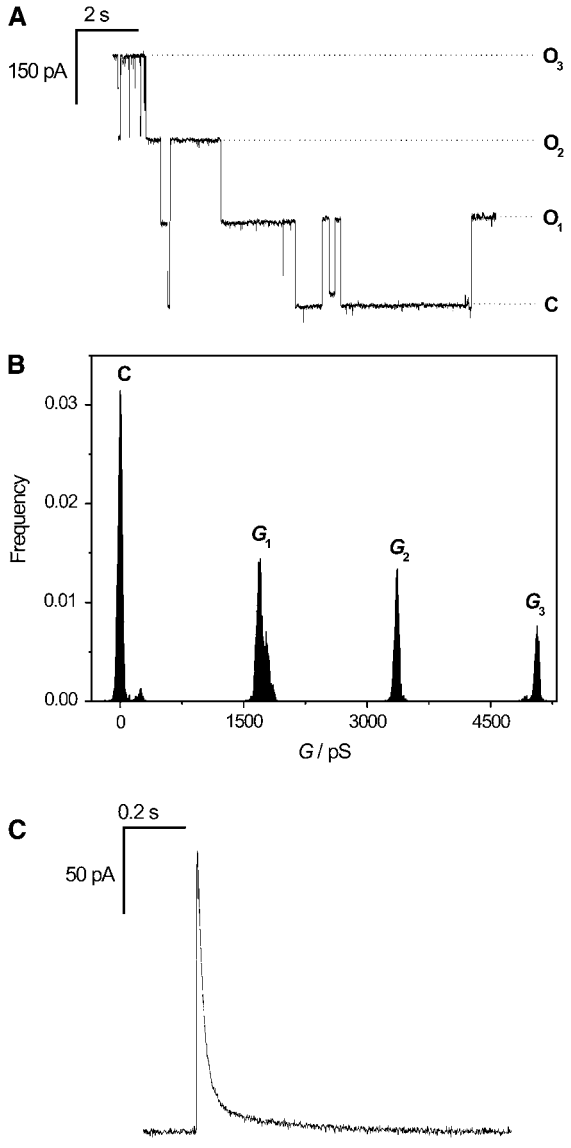


FIGURE 3 (*A*) Characteristic channel activity of one OmpF-trimer reconstituted in nano-BLMs at a holding potential of $U = -100$ mV. The current levels of the different opening states ($O_1$, $O_2$, $O_3$) and of the closed state (C) are indicated. (*B*) All-point histogram analysis of the current trace. The peaks represent the three conductance levels. The average conductance per monomer amounts to $G_m = 1690 \pm 20$ pS. (*C*) Transient current trace after OmpF insertion. Electrolyte, 1 M KCl, 1 mM $CaCl_2$, pH 6.0.

To obtain a mean value for the conductance of one subunit monomer of OmpF in nano-BLMs, an amplitude histogram composed of 583 events was generated with a bin width of 100 pS (Fig. 4). The conductance level of one subunit can be clearly assigned in the amplitude histogram. A Gaussian function was fit to the data in a range of 500–2500 pS, resulting in a mean conductance value of $G_1 = 1400 \pm 200$ pS. This conductance value is in good agreement with the observed conductance level of 1500 pS of a single monomer monitored under the same experimental conditions (41). The concerted opening of two or three subunits is expected to be in the range of 2000–6000 pS, where indeed many events were detected. However, an unambiguous assignment of a defined conductance level arising from the simultaneous opening of two or three subunits was not possible.

Previous studies demonstrated that the OmpF channel exhibited both relatively slow and fast conductance changes. The terms slow and fast kinetics have been established in literature (37,39) and are commonly used to describe the different gating mechanisms of OmpF. We report here that the fast kinetic conductance changes can also be observed in nano-BLMs. Fig. 5 *A* depicts a typical current trace with fast openings and closures of a single monomer superimposed on the slow kinetics of the channels. Such fast kinetics could be observed in ~30% of all events. The all-point histogram analysis of the data is shown in Fig. 5 *B*. The first and second conductance states are clearly split into two different levels. $G_1$ and $G_2$ can be assigned to the full opening of one and two OmpF subunits, respectively, with the characteristic monomer conductances of $G_1 = 1800 \pm 110$ pS and $G_2 = 3600 \pm 60$ pS. Most prominent is, however, the conductance state $G_1'$, which is a result of the fast kinetics with a reduced conductance of $G_1' = 1300 \pm 100$ pS. The second conductance state, $G_2'$, is 400 pS lower ($G_2' = 3200 \pm 60$ pS) than the conductance of the full open state of two OmpF subunits. It

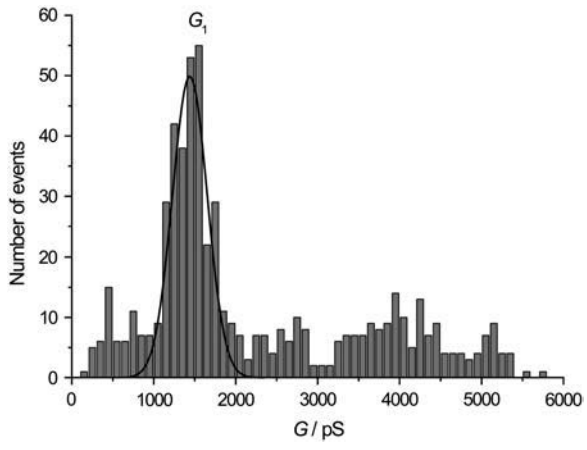


FIGURE 4 Amplitude histogram of 583 events (bin width 100 pS). A Gaussian function was fit to the data in the range of 500-2500 pS, resulting in a mean conductance value for a single monomer opening of $G_1 = 1400 \pm 200$ pS.

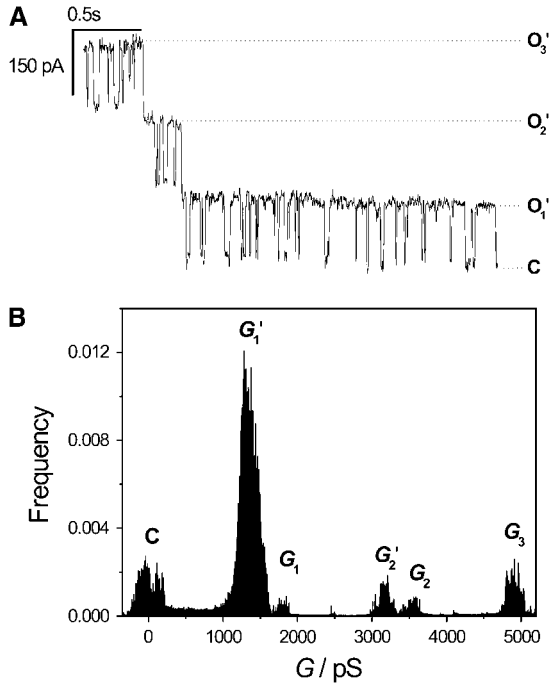


FIGURE 5 (*A*) Fast kinetics superimposed on slow channel activity of OmpF in nano-BLMs at $U = -100$ mV. The conductance of the short channel closure is slightly smaller than the slow kinetics. (*B*) All-point histogram of the current trace with multiple peaks caused by a smaller conductance of the fast events. Electrolyte, 1 M KCl, 1 mM $CaCl_2$, pH 6.0.

is important to note that the appearance of the traces is influenced by the sampling rate and the filtering frequency. We worked with a sampling rate of 50 kHz and a corner filter frequency of 1 kHz, which allows detecting kinetic details. However, one has to be aware of the fact that faster events might not be monitored because of the limited bandwidth.

Besides analyzing the fast kinetics in terms of conductivity, their length was determined and compared to those of the slow kinetics. Fig. 6 *A* illustrates the number of events as a function of their length: 502 events were compiled in the statistics with a bin width of 10 ms. A monoexponential decay function was fit to the data in a range of 0–150 ms, resulting in a time constant of $\tau = 20$ ms. In Fig. 6 *B* the duration of the slow kinetics is plotted with a bin width of 1 s. Most channel events exhibited a length of 1–10 s. The longest channel opening detected lasted 13 min, which implies that OmpF in the open state has resided within a membrane over a 60-nm-sized pore during this time period and did not diffuse across the pore rims, which would result in a transient current. This long opening is not displayed in the graph. Fitting a monoexponential function to the data results in a time constant of $\tau = 5.3$ s.

Basle et al. (39) reported on conductance levels of OmpF that are smaller than the monomer conductance, so-called subconductance states. We were also able to resolve OmpF activity of minor conductance in nano-BLMs, as displayed in Fig. 7 *A*. The subconductance level is well resolved in the

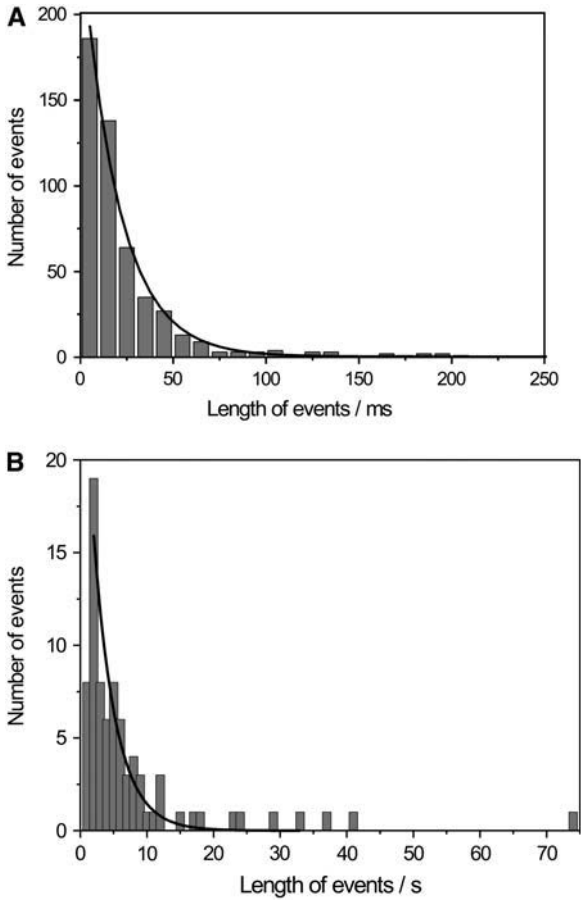


FIGURE 6 (*A*) Number of fast kinetic events as a function of their length (bin width 10 ms, 502 events). A monoexponential decay function (—) was fit to the data, leading to a time constant of $\tau = 20$ ms. (*B*) Statistics of the number of slow kinetic events (bin width 1 s, 80 events). The fit results in a time constant of $\tau = 5.3$ s. The longest event detected lasted 13 min and is not displayed in the graph. Electrolyte, 1 M KCl, 1 mM $CaCl_2$, pH 6.0.

corresponding histogram (Fig. 7 *B*), which allows for the determination of the conductivity $G_S = 320 \pm 100$ pS. The duration time of this particular event is 128 ms. Typically, the duration of a subconductance state was found to be in the range of 1–20 ms. If the duration of a subconductance state is very small, it is difficult to distinguish it from fast kinetics events. Such minor conductance levels were unambiguously observed in fewer than 10% of all events.

### Influence of ampicillin on channel activity

The monitored three-step opening and closure as well as the observed fast kinetics are characteristic properties of the OmpF channel activity and indicate a functional insertion of the protein into the nano-BLMs. Ampicillin is known to modify the gating of OmpF such that it transiently blocks the ion flow. The influence of ampicillin has been investigated by both computational and electrochemical methods in the last few years (41,43). With a time resolution of 15 $\mu$s it is

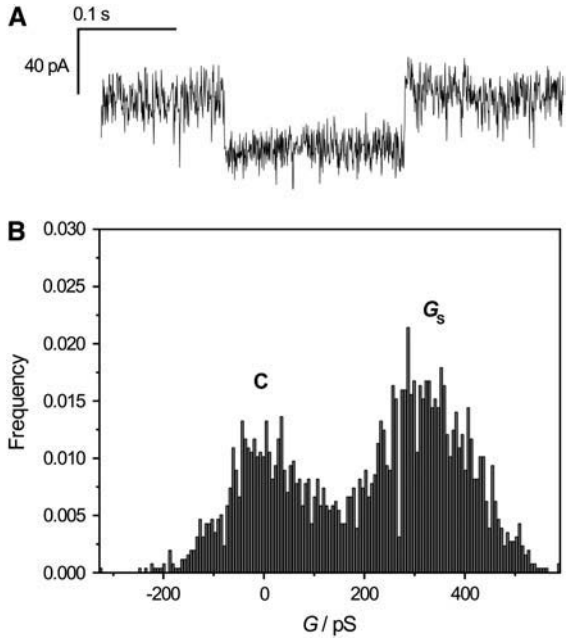


FIGURE 7 (*A*) Current trace displaying a subconductance state of OmpF gating in nano-BLMs. (*B*) All-points histogram of the current recording. The subconductance state is well resolved and exhibits a value of $G_S = 320 \pm 100$ pS. Electrolyte, 1 M KCl, 1 mM $CaCl_2$, pH 6.0.

possible to resolve fast single-molecule ampicillin binding to OmpF, whereas at a resolution of 150 $\mu$s blockage events were observed only as downward spikes. Our setup does not allow for such high temporal resolution. Assuming that the resolution is limited by the low-pass filter setting to 2 kHz, the rise time is 166 $\mu$s, which corresponds to the minimum length of a pulse to which the filter gives a nearly full-amplitude response. However, after adding 6 mM of ampicillin to the *cis* compartment, characteristic downward spikes interpreted as blockades of one OmpF monomer inserted in the pore-spanning membrane were observed (Fig. 8 *A*). In some of the events, an almost full blockade of one monomer was observed. At the end of the current trace the monomer completely switches to the closed state. In comparison, Fig. 8*B* depicts the channel activity in the absence of ampicillin. At the beginning of the current trace, a fast kinetic event is well resolved characterized by a current level of the closed state. The characteristic downward spikes that mark the influence of ampicillin are not present. Again, at the end of the current trace the channel closes.

## DISCUSSION

The development of artificial robust membrane systems that allow for the investigation of integral membrane proteins and ion channels has been subject to research for many years. To obtain such a system, we established membranes suspending the pores of a porous matrix as a hybrid of solid supported and free-standing bilayers (16–18). Starting with a porous

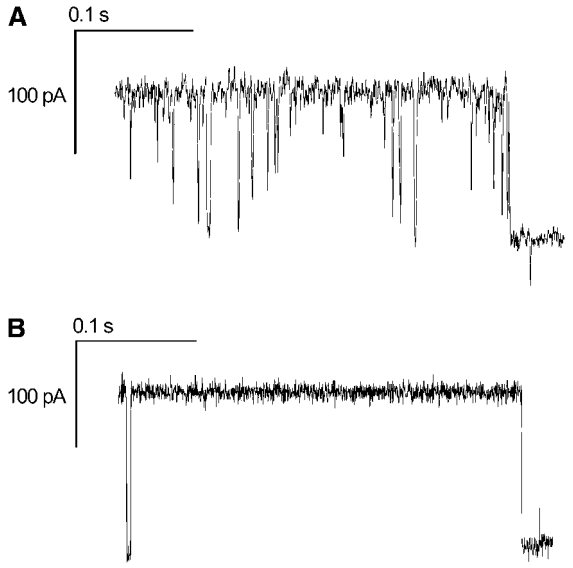


FIGURE 8 (*A*) Current recording for a single OmpF channel reconstituted in a nano-BLM in the presence of 6 mM ampicillin. The downward spikes represent the blockade of one monomer. (*B*) Current recording for a single OmpF channel reconstituted in a nano-BLM in the absence of ampicillin. The event at the beginning of the trace marks a fast gating event. Electrolyte, 1 M KCl, 1 mM $CaCl_2$, pH 6.0.

alumina substrate with a pore size of 60 nm, a lipid bilayer is formed after applying a lipid droplet of DPhPC dissolved in *n*-decane onto the DPPTE-functionalized upper surface. The bilayer formation process can be elucidated by monitoring the membrane capacitance, showing that the most significant change arises within the first minutes (17). To investigate the initial process in more detail here, the phase angle $\phi$ was followed time-resolved at a frequency of $10^6$ Hz, which turned out to be a convenient method to follow the success of the thinning process. The capacitance of a layer is inversely proportional to its thickness, which yields in small capacitance values for thick layers. A capacitive element causes a phase shift of $-90°$ between current and voltage. At $10^6$ Hz, a thick lipid-solvent droplet produces a phase angle of $-90°$ because its capacitance is small enough to be monitored at this high frequency. However, a fully formed thin lipid bilayer has a larger capacitance, which is monitored at frequencies $<10^5$ Hz. Thus, the electrolyte resistance exhibiting a phase angle of 0° dominates at $10^6$ Hz. Even though we do not know microscopically how thinning occurs in nano-BLMs, it might in part be similar to what has been observed in BLMs and solid-supported membranes. Tien and Dawidowicz (45) postulated a zipper-like mechanism for the thinning of BLMs generated by the Müller-Rudin technique. Initial bilayer areas induced by thermal motion or mechanical vibration drive the membrane formation along with the extrusion of solvent to the outer area, referred to as the Plateau-Gibbs border. Fujiwara et al. (46) were able to visualize this dynamic process by means of a long-distance microscope. They confirmed Tien's hypothesis of the zipper mechanism and furthermore stated that the initial bilayer areas need to exhibit a minimum size to promote the formation process. Otherwise remaining solvent will separate already existing bilayer areas through a phenomenon called the Marangoni effect. However, because nano-BLMs exhibit a multitude of pores with adjoining bilayers, which are separated by solid-supported membrane areas where the membrane is immobilized via the hydrophobic DPPTE-submonolayer, the formation of a Plateau-Gibbs border in every single pore is not very likely. However, on solid supports, thinning of a lipid bilayer obtained by the painting technique was also observed (47). After the application of a lipid-solvent droplet on a hydrophobic monolayer on gold, Florin and Gaub observed a rapid thinning process along with the extrusion of solvent. Excessive solvent remained on the substrate in a domain-like manner. As deduced from the rather low capacitances of $(0.4 \pm 0.1)$ $\mu F/cm^2$ of the nano-BLMs, residual solvent is very likely to be present in the membrane system. This is supported by the observation that in around 50% of all nano-BLM preparations, a sudden small drop of the phase angle was observed, which might be a result of the dynamics of residual solvent. Further investigation need to be performed to fully elucidate the mechanism of nano-BLM formation.

A detailed characterization of the electrical parameters of each nano-BLM preparation was performed by impedance spectroscopy and revealed that the obtained mean specific membrane capacitances of all nano-BLM preparations were in good agreement with values of BLMs generated by the Müller-Rudin-technique (44) taking the porous area of the porous material into account. Only the porous area is used for the calculation of the specific capacitance because of the assumption that the conductance underneath the supported membrane parts attached via a DPPTE-monolayer on the gold surface is negligible. Moreover, nano-BLMs provide a high membrane resistance of $>1$ G$\Omega$ over the entire experimental period of 8–10 h, which is sufficient to perform single-channel recordings as has been demonstrated by the insertion of channel peptides (17). Here, we addressed the question of whether a large transmembrane protein can be functionally reconstituted into membranes covering nanometer-sized pores. It has been demonstrated that a functional reconstitution of integral membrane proteins such as $\alpha$-hemolysin in a membrane suspending the pores of a porous silicon substrate with pore diameters of 1–5 $\mu$m is feasible (19). Favero et al. (20) managed to insert the glutamate receptor in membranes spanning nonordered pores in a polycarbonate foil with diameters of around 1 $\mu$m. In our system, the diameter of the apertures is smaller by a factor of 17–83 than the abovementioned pores. The difference in terms of pore diameter between our system (60 nm) and the porous material utilized by Favero et al. (1 $\mu$m) becomes even more apparent when the number of lipid molecules covering one pore is calculated. With the molecular surface area of one DPhPC molecule of 69 $Å^2$ (48) taken into account, one pore of the

porous alumina holds ~4100 lipid molecules, whereas an orifice of 1 $\mu$m diameter is covered by ~1,140,000 lipid molecules.

Despite this large difference in pore size, we succeeded in the functional insertion of the outer membrane protein OmpF, which occupies an area of around 80 nm$^2$ (21), in nano-BLMs. The characteristic three-step opening and closing of the pores of one trimer was observed, which had already been detected in early studies on OmpF reconstituted in BLMs (32) and was confirmed in publications following (30,49). The conductance of one monomer deduced from all-point ($G_m = 1690 \pm 20$ pS) and amplitude-histogram analysis ($G_1 = 1400 \pm 200$ pS) is in good agreement with the value of 1500 pS reported by Nestorovich et al. (41) obtained under the same experimental conditions. Monomeric events are most likely to occur. However, the concerted activity of two or three pores was also observed. Similar findings were made by Morgan et al. (50), who also ascribed the most frequent events to a single pore. Besides the characteristic trimeric activity, it has been reported that OmpF comprises fast kinetics on a much smaller time scale (23,32,37). We were able to resolve such fast kinetics with a typical conductance level of the fast events of 1300 ± 100 pS, which is slightly smaller than the value of the full monomer opening. Berrier et al. (37) investigated the fast gating of OmpF in more detail by means of the patch-clamp technique and also reported on a smaller conductivity of these events compared to the values found for a monomer. Only recently, a thorough description of these so-called subconductance states was provided by Basle et al. (39). Using nano-BLMs with a reconstituted OmpF channel, we were able to monitor such subconductance states. In contrast to measurements on classical BLMs, occasionally we observed transient currents (Fig. 3 *C*), when OmpF was inserted into a nano-BLM. One explanation might be found in the diffusion of the OmpF channel from the free-standing part to the solid supported part. It is also conceivable that a protein that is localized preferentially in the solid supported region leads to a transient current in case of channel opening.

In the context of drug development and screening, the understanding of the essential step of translocation of such molecules across the target membrane is of major importance. Here, we investigated the influence of the $\beta$-lactam antibiotic ampicillin on the channel activity of OmpF. Even though the time resolution of our system was not sufficient to fully resolve every single ampicillin blockade, as was demonstrated in the work of Nestorovich et al. (41), blockades of ampicillin were clearly detected as downward spikes of the ion flow during the opening of one monomer (Fig. 8 *A*).

## CONCLUSIONS

It has been shown that nano-BLMs on porous alumina substrates with pore diameters of 60 nm are well suited for the functional insertion of large transmembrane proteins such as OmpF. All characteristic channel activities such as the trimeric conductance steps on opening and closing of the three monomers, typical fast kinetics, and subconductance states were monitored, which indicates that the close proximity of immobilized lipid bilayers on the pore rims does not influence the ion channel activity. The influence of the antibiotic ampicillin on the channel activity of OmpF was proven, demonstrating the potential of this membrane system for the development of a drug-screening device.

We gratefully acknowledge financial support by the DFG (STE 884/5-1).

## REFERENCES

1. Müller, P., H. T. Rudin, H. T. Tien, and W. C. Wescott. 1963. Methods for the formation of single bimolecular lipid membranes in aqueous solution. *J. Phys. Chem. B.* 67:534–535.
2. Montal, M., and P. Müller. 1972. Formation of bimolecular membranes from lipid monolayers and a study of their electrical properties. *Proc. Natl. Acad. Sci. USA.* 69:3561–3566.
3. Wilk, S. J., M. Goryll, G. M. Laws, S. M. Goddnick, and T. J. Thornton. 2004. Teflon$^{TM}$-coated silicon apertures for supported lipid bilayer membranes. *Appl. Phys. Lett.* 85:3307–3309.
4. Pantoja, R., D. Sigg, R. Blunck, F. Bezanilla, and J. R. Heath. 2001. Bilayer reconstitution of voltage-dependent ion channels using a microfabricated silicon chip. *Biophys. J.* 81:2389–2394.
5. Cheng, Y., R. J. Bushby, S. D. Evans, P. F. Knowles, R. E. Miles, and S. D. Ogier. 2001. Single ion channel sensitivity in suspended bilayers on micromachined supports. *Langmuir.* 17:1240–1242.
6. Osborn, T. D., and P. Yager. 1995. Formation of planar solvent-free phospholipid bilayers by Langmuir-Blodgett transfer of monolayers to micromachined apertures in silicon. *Langmuir.* 11:8–12.
7. Fertig, N., R. H. Blick, and J. C. Behrends. 2002. Whole cell patch clamp recording performed on a planar glass chip. *Biophys. J.* 82:3056–3062.
8. Sackmann, E. 1996. Supported membranes: Scientific and practical applications. *Science.* 271:43–48.
9. Steinem, C., A. Janshoff, W.-P. Ulrich, M. Sieber, and H.-J. Galla. 1996. Impedance analysis of ion transport through gramicidin channels incorporated in solid supported lipid bilayers. *Bioelectrochem. Bioenerg.* 42:213–220.
10. Purrucker, O., H. Hillebrandt, K. Adlkofer, and M. Tanaka. 2001. Deposition of highly resistive lipid bilayer on silicon-silicon dioxide electrode and incorporation of gramicidin studied by ac impedance spectroscopy. *Electrochim. Acta.* 47:791–798.
11. Tien, H. T., R. H. Barish, L.-Q. Gu, and A. L. Ottowa. 1998. Supported bilayer lipid membranes as ion and molecular probes. *Anal. Sci.* 14:3–18.
12. Sinner, E.-K., and W. Knoll. 2001. Functional tethered membranes. *Curr. Opin. Chem. Biol.* 5:705–711.
13. Cornell, B. A., G. Krishna, P. D. Osman, R. D. Pace, and L. Wieczorek. 2001. Tethered-bilayer lipid membranes as a support for membrane-active peptides. *Biochem. Soc. Trans.* 29:613–617.
14. Atanasov, V., N. Knorr, R. S. Duran, S. Ingebrandt, A. Offenhäuser, W. Knoll, and I. Köper. 2005. Membrane on a chip: a functional tethered lipid bilayer membrane on silicon oxide surfaces. *Biophys. J.* 89:1780–1788.
15. Terrettaz, S., M. Mayer, and H. Vogel. 2003. Highly electrically insulating tethered lipid bilayers for probing the function of ion channel proteins. *Langmuir.* 19:5567–5569.
16. Römer, W., Y. H. Lam, D. Fischer, A. Watts, W. B. Fischer, P. Göring, R. B. Wehrspohn, U. Gösele, and C. Steinem. 2004. Channel activity of a viral transmembrane peptide in micro-BLMs: $Vpu_{1–32}$ from HIV-1. *J. Am. Chem. Soc.* 126:16267–16274.

17. Römer, W., and C. Steinem. 2004. Impedance analysis and single-channel recordings on nano-black lipid membranes based on porous alumina. *Biophys. J.* 86:955–965.

18. Horn, C., and C. Steinem. 2005. Photocurrents generated by bacteriorhodpsin adsorbed on nano-black lipid membranes. *Biophys. J.* 89: 1046–1054.

19. Hemmler, R., G. Böse, R. Wagner, and R. Peters. 2005. Nanopore unitary permeability measured by electrochemical and optical single transporter recording. *Biophys. J.* 88:4000–4007.

20. Favero, G., L. Campanella, S. Cavallo, A. D'Annibale, M. Perella, E. Mattei, and T. Ferri. 2005. Glutamate receptor incorporated in a mixed hybrid bilayer lipid membrane array, as a sensing element of a biosensor working under flowing conditions. *J. Am. Chem. Soc.* 127: 8103–8111.

21. Cowan, S. W., T. Schirmer, G. Rummel, M. Steiert, R. Ghosh, R. A. Pauptit, J. N. Jansonius, and J. P. Rosenbusch. 1992. Crystal structures explain functional properties of two *E. coli* porins. *Nature.* 358:727–733.

22. Buehler, L. K., S. Kusumoto, H. Zhang, and J. P. Rosenbusch. 1991. Plasticity of *Escherichia coli* porin channels. Dependence of their conductance on strain and lipid environment. *J. Biol. Chem.* 266: 24446–24450.

23. Danelon, C., A. Suenaga, M. Winterhalter, and I. Yamato. 2003. Molecular origin of the cation selectivity in OmpF porin: single channel conductances vs. free energy calculation. *Biophys. Chem.* 104: 591–603.

24. Saint, N., K.-L. Lou, C. Widmer, M. Luckey, T. Schirmer, and J. P. Rosenbusch. 1996. Structural and functional characterization of OmpF porin mutants selected for larger pore size. *J. Biol. Chem.* 271:20676–20680.

25. Tieleman, D. P., and H. J. Berendsen. 1998. A molecular dynamics study of the pores formed by *Escherichia coli* OmpF porin in a fully hydrated palmitoyloleoylphosphatidylcholine bilayer. *Biophys. J.* 74: 2786–2801.

26. Im, W., and B. Roux. 2002. Ions and counterions in a biological channel: a molecular dynamics simulation of OmpF porin from *Escherichia coli* in an explicit membrane with 1 M KCl aqueous salt solution. *J. Mol. Biol.* 319:1177–1197.

27. Bredin, J., N. Saint, M. Mallea, E. De, G. Molle, J. M. Pages, and V. Simonet. 2002. Alteration of pore properties of *Escherichia coli* OmpF induced by mutation of key residues in anti-loop 3 region. *Biochem. J.* 363:521–528.

28. Miedema, H., A. Meter-Arkema, J. Wierenga, J. Tang, B. Eisenberg, W. Nonner, H. Hektor, D. Gillespie, and W. Meijberg. 2004. Permeation properties of an engineered bacterial OmpF porin containing the EEEE-locus of $Ca^{2+}$ channels. *Biophys. J.* 87:3137–3147.

29. Todt, J. C., W. J. Rocque, and E. J. McGroarty. 1992. Effects of pH on bacterial porin function. *Biochemistry.* 31:10471–10478.

30. Lakey, J. H., and F. Pattus. 1989. The voltage-dependent activity of *Escherichia coli* porins in different planar bilayer reconstitutions. *Eur. J. Biochem.* 186:303–308.

31. Nestorovich, E. M., and S. M. Bezukov. 2003. Residue ionization and ion transport through OmpF channels. *Biophys. J.* 85:3718–3729.

32. Schindler, H., and J. P. Rosenbusch. 1978. Matrix protein from *Escherichia coli* outer membrane forms voltage-controlled channels in lipid bilayers. *Proc. Natl. Acad. Sci. USA.* 75:3751–3755.

33. Xu, G. Z., B. Shi, E. J. McGroarty, and H. T. Tien. 1986. Channel-closing activity of porins from *Escherichia coli* in bilayer lipid membranes. *Biochim. Biophys. Acta.* 862:57–64.

34. Delcour, A. H., B. Martinac, J. Adler, and C. Kung. 1989. Voltage-sensitive ion channel of *Escherichia coli*. *J. Membr. Biol.* 112:267–275.

35. Robertson, K. M., and D. P. Tieleman. 2002. Molecular basis of voltage gating of OmpF porin. *Biochem. Cell Biol.* 80:517–523.

36. Van Gelder, P., F. Dumas, and M. Winterhalter. 2000. Understanding the function of bacterial outer membrane channels by reconstitution into black lipid membranes. *Biophys. Chem.* 85:153–167.

37. Berrier, C., A. Coulombe, C. Houssin, and A. Ghazi. 1992. Fast and slow kinetics of porin channels from *Escherichia coli* reconstituted into giant liposomes and studied by patch-clamp. *FEBS Lett.* 306: 251–256.

38. Delcour, A. H. 1997. Function and modulation of bacterial porins: insights from electrophysiology. *FEMS Microbiol. Lett.* 151:115–123.

39. Basle, A., R. Iyer, and A. H. Delcour. 2004. Subconductance states in OmpF gating. *Biochim. Biophys. Acta.* 1664:100–107.

40. Iyer, R., and A. H. Delcour. 1997. Complex inhibition of OmpF and OmpC bacterial porins by polyamines. *J. Biol. Chem.* 272:18595–18601.

41. Nestorovich, E. M., C. Danelon, M. Winterhalter, and S. M. Bezrukov. 2002. Designed to penetrate: time-resolved interaction of single antibiotic molecules with bacterial pores. *Proc. Natl. Acad. Sci. USA.* 99:9789–9794.

42. Iyer, R., Z. Wu, P. M. Woster, and A. H. Delcour. 2000. Molecular basis for the polyamine-OmpF porin interactions: inhibitor and mutant studies. *J. Mol. Biol.* 297:933–945.

43. Ceccarelli, M., C. Danelon, A. Laio, and M. Parrinello. 2004. Microscopic mechanism of antibiotics translocation through a porin. *Biophys. J.* 87:58–64.

44. Benz, R., O. Fröhlich, P. Läuger, and M. Montal. 1975. Electrical capacity of black lipid films and of lipid bilayers made from monolayers. *Biochim. Biophys. Acta.* 394:323–334.

45. Tien, H. T., and E. A. Dawidowicz. 1966. Black lipid films in aqueous media: a new type of interfacial phenomenon. Experimental techniques and thickness measurements. *J. Colloid Interface Sci.* 22: 438–453.

46. Fujiwara, H., M. Fujihara, and T. Ishiwata. 2003. Dynamics of the spontaneous formation of a planar phospholipid bilayer. *J. Chem. Phys.* 119:6768–6775.

47. Florin, E.-L., and H. E. Gaub. 1993. Painted supported lipid membranes. *Biophys. J.* 64:375–383.

48. Pownall, H. J., Q. Pao, H. L. Brockman, and J. B. Massey. 1987. Inhibition of lecithin-cholesterol acyltransferase by diphytanoyl phosphatidylcholine. *J. Biol. Chem.* 262:9033–9036.

49. Rostovtseva, T. K., E. M. Nestorovich, and S. M. Bezrukov. 2002. Partitioning of differently sized poly(ethylene glycol)s into OmpF porin. *Biophys. J.* 82:160–169.

50. Morgan, H., J. T. Lonsdale, and G. Alder. 1990. Polarity-dependent voltage-gated porin channels from *Escherichia coli* in lipid bilayer membranes. *Biochim. Biophys. Acta.* 1021:175–181.